

GHI: Graphormer over Conditioned Hypergraph Incidence for Aspect-Based Sentiment Analysis

Yu Du

Qiqihar University
2025936317@qqhru.edu.cn

Wenlong Zhu

Qiqihar University
zw1_qqhr@qqhru.edu.cn

Xingze Li

Qiqihar University
2025936326@qqhru.edu.cn

Chenglong Cao

Qiqihar University
2025936311@qqhru.edu.cn

Jing Wang

Qiqihar University
2025912341@qqhru.edu.cn

Yukun Ma

Qiqihar University
2024935328@qqhru.edu.cn

Abstract

Aspect-based sentiment analysis (ABSA) requires models to bind sentiment evidence to the correct aspect, making it a natural testbed for fine-grained structural reasoning. We introduce GHI, a Graphormer-over-Conditioned-Hypergraph-Incidence framework that is designed as an incidence-based structural reasoning layer built on a bipartite topology. GHI represents diverse linguistic and semantic evidence as token–hyperedge incidence relations, allowing different structural signals to be incorporated through a unified interface. Extensive experiments on six standard ABSA benchmarks show that GHI outperforms all baselines on the SemEval domains, and multi-seed evaluations show stable improvements over strong DeBERTa. Further experiments show that with only 247M parameters, GHI approaches the performance of 11B Flan-T5 based methods on the ISE benchmark. Moreover, it demonstrates strong robustness on the challenging ARTS datasets, maintaining highly competitive performance where traditional models degrade. These results demonstrate that compact structural reasoning remains a valuable alternative to scale-driven approaches for fine-grained tasks.

1 Introduction

Aspect-Based Sentiment Analysis (ABSA) aims to predict the sentiment polarity toward a given aspect term or target entity (Zhang et al., 2023). Unlike sentence-level sentiment classification, ABSA is a fine-grained evidence-binding task that requires the model to separate different opinion clues within the same sentence. For example, as shown in Figure 1, the sentence expresses a positive sentiment "great" towards "GPU" while expressing a negative sentiment "expensive" towards "price", requiring the model to bind each opinion cue to correct aspect.

More fundamentally, to further distinguish different evidence-binding patterns, ABSA needs diverse complex structural representations from different

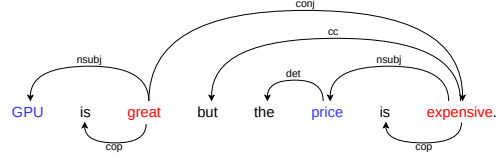


Figure 1: An example sentence with two different aspects (colored in blue) and opinion evidences (colored in red). The sentence has already been preprocessed by its dependency parser.

directions. In the local-context direction, Zeng et al. (2019) constrain attention to aspect-centered windows, making the model focus on nearby opinion words. Recent fusion-based models further combine semantic attention with syntactic structure, for example, Jin et al. (2025) use Aspect-NA and adaptive hierarchical cross-attention to integrate semantic and dependency-aware features. Another direction focuses mainly on graph structures. Specifically, Yin and Zhong (2024) couple graph-view message passing with sequence-view Transformer modeling, jointly capturing syntactic connectivity and semantic interactions.

Viewed across existing methods, ABSA methods that introduce high-order relations or inject complex structures can be seen as helping the model identify and organize the aspect-relevant evidence. Moreover, most of them design each source of evidence in isolated views. This observation motivates a general question: can ABSA benefit from a common structural framework through which diverse evidence can be represented, extended, and reasoned over?

To make this picture clear, we need a structure that possesses both the capability for multiple representations and scalability. For this reason, hypergraphs provide a natural candidate (Feng et al., 2019). As illustrated in Figure 2, their hyperedge design enables heterogeneous groups of tokens to be connected under a shared evidence unit, and the

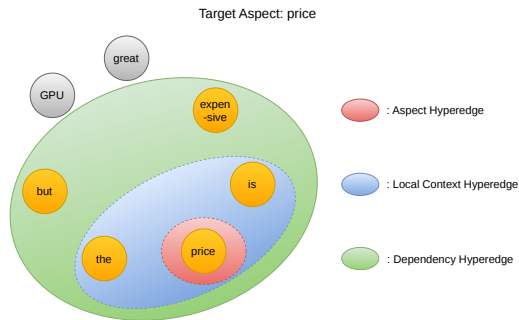


Figure 2: A hypergraph view for the aspect "price". Each colored ellipse denotes a hyperedge that connects multiple tokens as one evidence unit.

structural properties inherited from graphs make them extensible to new sources. Meanwhile, recent studies attempt to construct word-level relational hypergraphs to model high-order relations for ABSA, further showing their potential for high-order reasoning (Ouyang et al., 2024a; Ju et al., 2025; Kashyap et al., 2025).

However, to model such a complex structure, there remains a lack of effective ways to integrate multi-level information. Another straightforward challenge is that it is typically difficult to modify a graph structure when attempting to incorporate new knowledge. Fortunately, previous works have demonstrated the potential of both global attention and dynamic scalability on complex graph structures. For instance, Ying et al. (2021) proposed Graphormer, which utilizes the shortest path distance (SPD) between nodes to enable global attention for complex graph structure. In parallel, within the computer vision domain, Lei et al. (2025) introduced the concept of HyperACE. This work demonstrates how adaptive hyperedge mechanisms operate in practice, offering fresh insights into the scalability of hypergraphs.

Building upon these advancements, we propose GHI, a Graphormer-over-Hypergraph-Incidence framework for ABSA. GHI expresses multiple evidence as token-hyperedge incidence relations, so that different structural signals can be incorporated through a unified interface while keeping the downstream reasoning layer unchanged. In our ABSA instantiation, GHI uses a small set of canonical ABSA priors, including aspect spans, aspect-relative local regions, and dependency neighborhoods, and complements them with context-conditioned adaptive hyperedges for

sample-specific latent evidence. In addition, by lifting hyperedges into explicit nodes, GHI performs Graphormer-style reasoning over a bipartite star-expanded token-hyperedge graph.

In summary, the main contributions of our work are as follows:

- We propose GHI, an incidence-based structural reasoning framework for ABSA. GHI represents linguistic and semantic evidence as token-hyperedge incidence relations, providing a unified interface that can naturally accommodate different structural signals without source-specific reasoning branches.
- We introduce a bipartite star-expanded Graphormer built on a static-adaptive hypergraph design. By lifting diverse evidence into explicit reasoning nodes, GHI turns token-hyperedge incidence relations into a bipartite topology and applies Graphormer-style global attention over it.
- We conduct comprehensive evaluations on standard ABSA benchmarks, implicit sentiment evaluation (ISE), and adversarial robustness tests (ARTS). Results show that GHI outperforms strong baselines while exhibiting robust performance against complex linguistic variations.

2 Methodology

2.1 Overview

We propose **GHI**, a **Graphormer-over-Conditioned Hypergraph Incidence** framework for ABSA. GHI lifts structural priors and adaptive semantic clusters into explicit nodes, thereby forming a bipartite star-expanded graph for global Graphormer attention (indicated by the purple arrows). As illustrated in Figure 3, the framework operates as a unified incidence-level routing layer, where distinct colors differentiate the diverse evidence sources.

Specifically, GHI constructs static hyperedges for deterministic linguistic evidence and adaptive hyperedges conditioned on contextual anchors. With both soft and hard Top- K incidence views, the soft incidence supports differentiable token-hyperedge propagation, while the hard Top- K incidence instantiates a sparse star-expanded topology for Graphormer reasoning with structural biases.

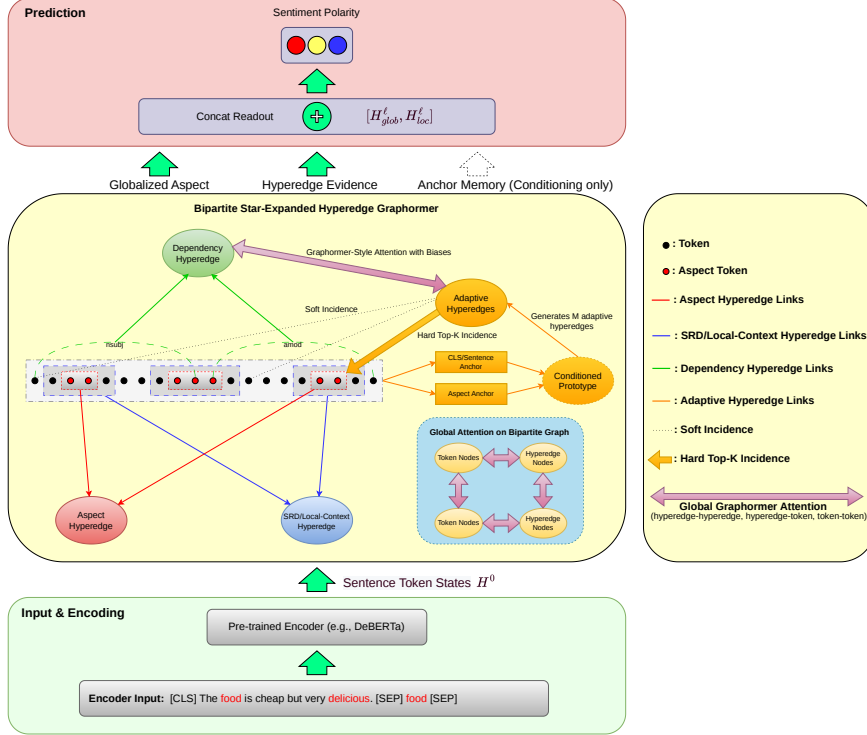


Figure 3: The overall architecture of the proposed GHI framework. Static ABSA priors, including aspect (red), SRD/local-context (blue), and dependency (green) hyperedges, are color-coded by source and represented together with adaptive hyperedges in a token–hyperedge incidence structure. Dotted lines denote soft incidence weights used for token–hyperedge propagation, while orange Top- K links define the sparse hard incidence topology. The purple bidirectional arrows indicate Graphormer-style global attention over the entire bipartite token–hyperedge graph.

2.2 Task Formulation and Encoding

Given an aspect span $a = [l, r)$ within a sequence $x = [x_1, \dots, x_N]$, and a sentiment label $y \in \mathcal{Y}$, ABSA aims to predict the sentiment polarity expressed toward the given aspect. For pre-trained encoders, the sentence–aspect pair is used as the input, while only the contextual states of the original sentence tokens are retained as H^0 for graph reasoning. We encode the sentence–aspect pair to obtain contextual representations:

$$H^0 = [h_1^0, \dots, h_N^0] = \text{Enc}(x, a), \quad (1)$$

where $H^0 \in \mathbb{R}^{N \times d}$, and the half-open span $[l, r)$ denotes the target aspect tokens from x_l to x_{r-1} .

Graph reasoning operates solely on valid sentence tokens. With a binary mask $m \in \{0, 1\}^N$, the sentence anchor is initialized as $c^0 = \text{Pool}_m(H^0)$ with mean pooling $\text{Pool}_m(\cdot)$ over valid tokens, and the aspect anchor is initialized as $a^0 = \text{Pool}_{[l,r)}(H^0)$ with mean pooling $\text{Pool}_{[l,r)}(\cdot)$ over the target aspect span.

2.3 Conditioned Hypergraph Incidence

The core of GHI is a conditioned hypergraph incidence representation. At layer ℓ , we define a hypergraph $\mathcal{G}^\ell = (V, \mathcal{E}^\ell, I^\ell)$ over the current token states H^ℓ , where V is the set of token nodes, \mathcal{E}^ℓ is the set of hyperedges, and $I^\ell \in \mathbb{R}^{|V| \times |\mathcal{E}^\ell|}$ is the token–hyperedge incidence matrix. GHI combines task-informed static hyperedges with context-conditioned adaptive hyperedges. The sentence and aspect anchors are maintained as layer-wise memories, after each reasoning layer ℓ , they are updated by gated MLPs as $c^{\ell+1}, a^{\ell+1} = \text{AnchorUpdate}(c^\ell, a^\ell, H^{\ell+1})$, where $\text{AnchorUpdate}(\cdot)$ denotes gated MLP updates over the aspect-level pooled regions.

Static Hyperedges We first construct a binary incidence matrix I^{sta} from three static hyperedge priors. The aspect hyperedge e_{asp} connects all tokens inside the target span: $e_{\text{asp}} = \{i \mid l \leq i < r\}$. To encode aspect-centered local context, we follow Zeng et al. (2019) and compute the semantic-relative distance (SRD) $d_i = \max(0, |i - \frac{l+r-1}{2}| - \lfloor \frac{r-l}{2} \rfloor)$. This prior is then instantiated as a local-

context hyperedge e_{srd} that connects tokens within a radius ρ : $e_{\text{srd}} = \{i \mid m_i = 1, d_i \leq \rho\}$. Then, the dependency hyperedge e_{dep} collects tokens reachable from aspect tokens within T hops on the dependency graph: $e_{\text{dep}} = \{i \mid m_i = 1, \text{dist}_{\text{dep}}(i, e_{\text{asp}}) \leq T\}$. Word-level dependency edges are projected to subwords to align with encoder outputs. Taken together, these priors form a static incidence matrix $I^{\text{sta}} \in \mathbb{R}^{|V| \times S}$, where S denotes the number of static hyperedges.

Adaptive Hyperedges Static hyperedges provide reliable task priors, but they cannot cover all sample-specific opinion patterns. To complement them, GHI induces a small set of adaptive hyperedges at each layer, conditioned on the locally refined token states and current anchor memories c^ℓ and a^ℓ . As illustrated in the upper-right part of Figure 3, the adaptive hyperedge prototypes generate M adaptive hyperedges, and further form a soft token–hyperedge incidence matrix $I_{\text{ad}}^\ell \in \mathbb{R}^{|V| \times M}$:

$$I_{\text{ad}}^\ell = \text{AdaptiveIncidence}(\tilde{H}^\ell, c^\ell, a^\ell), \quad (2)$$

where $\text{AdaptiveIncidence}(\cdot)$ denotes the adaptive incidence generator. Its prototype-based parameterization is given in Appendix B.1.

The adaptive incidence is concatenated with static incidence matrix to support differentiable token–hyperedge propagation, generally forming a soft incidence matrix $I_{\text{soft}}^\ell \in \mathbb{R}^{|V| \times (S+M)} = [I^{\text{sta}}, I_{\text{ad}}^\ell]$. Meanwhile, we retain the Top- K tokens for each adaptive hyperedge to obtain a sparse hard incidence matrix $I_{\text{hard}}^\ell \in \mathbb{R}^{|V| \times (S+M)} = [I^{\text{sta}}, \text{TopK}(I_{\text{ad}}^\ell)]$, which instantiates the bipartite star-expanded topology used by Graphormer reasoning.

2.4 GHI Reasoning Layer

GHI stacks L reasoning layers over the conditioned incidence structure. A layer-wise computation flow is provided in Appendix B.2. By treating both tokens and hyperedges as explicit reasoning nodes, each layer couples two complementary views of token–hyperedge reasoning: the soft incidence view supports differentiable propagation over graded token–hyperedge memberships, while the hard incidence view instantiates a sparse token–hyperedge bipartite topology. This star-expanded graph allows Graphormer-style attention to model token–token, token–hyperedge, and hyperedge–

hyperedge interactions within a shared structural space.

Local Context Refinement Before constructing adaptive incidence, GHI applies a local-window self-attention to refine short-range token interactions. Given the graph-visible mask m and window size w , $\text{LocalAttn}(\cdot)$ restricts multi-head self-attention to token pairs (i, j) satisfying $m_i = m_j = 1$ and $|i - j| \leq w$. The local refinement is written as: $\tilde{H}^\ell = H^\ell + \text{LocalAttn}(\text{LN}(H^\ell), m, w)$. The locally refined states \tilde{H}^ℓ then guide the adaptive hyperedge incidence described in Section 2.3.

Incidence-Aware Hypergraph Reasoning Given the soft incidence matrix I_{soft}^ℓ , GHI summarizes token information into hyperedge states through incidence-weighted pooling:

$$Z^\ell = \text{EdgePool}(\tilde{H}^\ell, I_{\text{soft}}^\ell). \quad (3)$$

Here, $\text{EdgePool}(\cdot)$ aggregates token states according to their soft token–hyperedge participation weights and adaptive priors.

We denote the resulting incidence-aware local token representation as H_{loc}^ℓ . It is obtained by two complementary operations. $\text{HGRefine}(\cdot)$ first performs soft token–hyperedge propagation and writes hyperedge messages back to tokens, while $\text{Relation-Aware Incidence Attention IncAttn}(\cdot)$ applies token–hyperedge attention using incidence-level relation features Φ^ℓ :

$$H_{\text{loc}}^\ell = \tilde{H}^\ell + \text{HGRefine}(\tilde{H}^\ell, Z^\ell, I_{\text{soft}}^\ell) + \text{IncAttn}(\tilde{H}^\ell, Z^\ell, I_{\text{soft}}^\ell, \Phi^\ell) \quad (4)$$

Specifically, Φ^ℓ includes edge type, edge role (static or adaptive), incidence weight, and SRD.

Star-Expanded Graphormer Reasoning While the soft incidence view supports differentiable hypergraph propagation, GHI also uses the hard incidence view I_{hard}^ℓ to construct a sparse star-expanded graph. The expanded graph contains both token nodes and hyperedge nodes. A token node is connected to a hyperedge node if the corresponding hard incidence entry is non-zero. The node states of the star-expanded graph are initialized as $X^\ell = [\tilde{H}^\ell; Z^\ell]$.

Following the Graphormer design (Ying et al., 2021), we extract structural encodings from the

expanded graph, including topological connectivity and pairwise relation types, and inject them as Graphormer structural biases for multi-head self-attention. In this way, global attention is aware of token–token, token–hyperedge, and hyperedge–hyperedge relations within the bipartite topology. The global update is written compactly with layer normalization (LN):

$$X_{\text{glob}}^{\ell} = X^{\ell} + \text{GraphormerAttn}(\text{LN}(X^{\ell}), \mathcal{B}^{\ell}), \quad (5)$$

where \mathcal{B}^{ℓ} denotes the Graphormer structural biases derived from the hard incidence topology I_{hard}^{ℓ} . We then split the output back into token and hyperedge parts:

$$X_{\text{glob}}^{\ell} = [H_{\text{glob}}^{\ell}; Z^{\ell+1}], \quad (6)$$

where H_{glob}^{ℓ} denotes the global token representation produced by the star-expanded Graphormer.

Local-Global Fusion GHI fuses the local evidence H_{loc}^{ℓ} and the star-expanded global token representation conditioned on the sentence and aspect anchors:

$$U^{\ell} = \text{Fuse}(H_{\text{glob}}^{\ell}, H_{\text{loc}}^{\ell}, c^{\ell}, a^{\ell}). \quad (7)$$

The next-layer token states are then produced by a residual feed-forward update: $H^{\ell+1} = U^{\ell} + \text{FFN}(\text{LN}(U^{\ell}))$.

2.5 Prediction and Training

After L reasoning layers, GHI predicts sentiment polarity from local readout derived from H_{loc}^{ℓ} and global readout derived from H_{glob}^{ℓ} . Two readouts are concatenated and passed to a linear classifier to obtain $p(y | x, a)$. Notably, in our main configuration, the anchor memory is used for conditioning incidence induction and local-global fusion U^{ℓ} , but is not included in the final readout. The entire training is with the standard cross-entropy loss:

$$\mathcal{L} = -\log p(y | x, a), \quad (8)$$

3 Experiments

We conduct experiments under a unified evaluation protocol. Unless otherwise specified, we use the standard train / test splits and report Accuracy and Macro-F1. We also conduct hyperparameter sensitivity analyses in Appendix C. All experimental details are provided in Appendix A.

3.1 Main Results

Table 1 reports the overall performance of GHI alongside previous state-of-the-art models across six benchmark datasets. GHI particularly outperforms all baselines on the SemEval domains. Driven by the DeBERTa encoder (He et al., 2020), the proposed framework yields 90.97% / 86.40% of Accuracy / Macro-F1 on Restaurant14 and 86.08% / 83.74% on Laptop. Notably, GHI outperforms knowledge-augmented baselines such as AGCL (Jian et al., 2025), suggesting that incidence-based structural modeling can also provide gains complementary to external augmentation. Furthermore, GHI maintains competitive performance on multi-domain datasets, including Twitter and the challenging MAMS benchmark. Overall, GHI shows strong gains on the SemEval domains and remains comparable to strong baselines on Twitter and MAMS.

3.2 Controlled Encoder Comparison

Previous studies have highlighted reproducibility issues and evaluation instability in ABSA evaluation, showing that random seeds, encoder capacities, and implementation details can noticeably affect reported performance (Dai et al., 2021; Mukherjee et al., 2021; Yang et al., 2023). To address these concerns, we evaluate GHI alongside representative structural models under identical BERT-base and DeBERTa-base encoders across multiple random seeds, aiming to separate structural gains from encoder capacity and training variance.

Table 2 presents the controlled evaluation results. We strictly adhere to the hyperparameter configurations recommended in the original papers, and use the multi-seed setting to observe relative improvements under the same encoder constraints. Under these conditions, GHI yields stable and substantial gains. Specifically, it improves Accuracy / Macro-F1 by 1.00% / 1.91% on Restaurant14 and 1.39% / 1.85% on Laptop relative to the strong vanilla DeBERTa baseline. Furthermore, GHI maintains competitive performance when compared to other state-of-the-art models under the same encoder constraints. These results verify that the gains of GHI are not merely attributable to encoder capacity or training variance, but are consistent with the benefits of its incidence-based reasoning design.

Model	Encoder	Restaurant14		Laptop		Twitter		Restaurant15		Restaurant16		MAMS	
		Acc	F1	Acc	F1	Acc	F1	Acc	F1	Acc	F1	Acc	F1
SK-GCN(Zhou et al., 2020)	BERT	83.48	75.19	79.00	75.57	75.00	73.01	83.20	66.78	87.19	72.02	-	-
KumaGCN(Chen et al., 2020)	BERT	86.43	80.30	81.98	78.81	77.89	77.03	86.35	70.76	92.53	79.24	-	-
R-GAT(Wang et al., 2020)	BERT	86.60	81.35	78.21	74.07	76.15	74.88	-	-	-	-	84.52	83.74
DGEDT(Tang et al., 2020)	BERT	86.30	80.00	79.80	75.60	77.90	75.40	84.00	71.00	91.90	79.00	-	-
DualGCN(Li et al., 2021a)	BERT	87.13	81.16	81.80	78.10	77.40	76.02	-	-	-	-	-	-
TGCN(Tian et al., 2021)	BERT	86.16	79.95	80.88	77.03	76.45	75.25	85.26	71.69	92.32	77.29	83.38	82.77
SSEGCN(Zhang et al., 2022)	BERT	87.31	81.09	81.01	77.96	77.40	76.02	-	-	-	-	-	-
dotGCN(Chen et al., 2022)	BERT	86.16	80.49	81.03	78.10	78.11	77.00	85.24	72.74	93.18	<u>82.32</u>	84.95	84.44
MWGCN(Yu and Zhang, 2023)	BERT	86.36	80.54	79.78	76.68	75.00	74.30	85.61	72.88	82.05	79.21	-	-
APARN(Ma et al., 2023)	BERT	87.76	82.44	81.96	79.10	79.76	78.79	-	-	-	-	85.59	85.06
DAGCN(Wang et al., 2024)	BERT	88.03	82.64	82.59	79.40	78.73	78.01	-	-	-	-	85.25	84.87
S ² GSL(Chen et al., 2024)	BERT	87.31	82.84	82.46	79.07	77.84	77.11	-	-	-	-	85.17	84.74
TextGT(Yin and Zhong, 2024)	BERT	87.31	82.27	81.33	78.71	77.70	76.45	-	-	92.21	81.48	-	-
MLFM(Jin et al., 2025)	BERT	87.31	82.50	82.12	79.06	77.55	76.83	-	-	-	-	-	-
PWCN [†] (Zhang et al., 2019)	RoBERTa	87.35	80.85	84.01	81.08	77.02	75.52	-	-	-	-	-	-
SARL(Wang et al., 2021)	RoBERTa	88.21	82.44	<u>85.42</u>	<u>82.97</u>	78.03	76.97	<u>88.19</u>	<u>73.83</u>	<u>94.62</u>	81.92	-	-
PCov(Feng et al., 2023)	RoBERTa	89.29	84.27	83.54	80.89	78.47	77.53	-	-	-	-	<u>85.55</u>	<u>85.05</u>
DAGF(Ji et al., 2026)	RoBERTa	89.37	84.37	83.07	80.38	77.25	76.55	-	-	-	-	-	-
RCL(Jian et al., 2024)	DeBERTa	89.38	84.68	82.76	80.28	78.32	77.47	-	-	-	-	-	-
AGCL [‡] (Jian et al., 2025)	DeBERTa	<u>90.30</u>	<u>85.63</u>	84.54	82.15	<u>78.85</u>	<u>78.15</u>	-	-	-	-	-	-
GHI(ours)	DeBERTa	90.97	86.40	86.08	83.74	78.73	77.72	90.22	79.37	95.29	87.84	84.96	84.42

Table 1: Overall performance on six ABSA benchmark datasets. Best results are in bold and second-best are underlined. † indicates result retrieved from Dai et al. (2021), while others are from their original papers. ‡ denotes that AGCL (Jian et al., 2025) utilizes a frozen DeBERTa-Large encoder rather than the base version.

Encoder	Model	Restaurant14		Laptop	
		Acc	F1	Acc	F1
BERT _{base}	BERT	85.65(0.61)	79.13(1.21)	78.39(0.67)	74.72(0.73)
	DAGCN	86.17(0.42) _{↑0.52}	79.59(0.80) _{↑0.46}	80.36(0.46) _{↑1.97}	76.90(0.67) _{↑2.18}
	TextGT	86.38(0.44) _{↑0.73}	80.39(0.70) _{↑1.26}	80.70(0.64) _{↑2.31}	77.65(0.86) _{↑2.93}
	MLFM	86.23(0.48) _{↑0.58}	79.93(0.71) _{↑0.80}	80.47(0.56) _{↑2.08}	76.92(0.90) _{↑2.20}
	GHI(ours)	86.06(0.99) _{↑0.41}	80.30(1.13) _{↑1.15}	79.59(0.79) _{↑1.20}	76.11(0.90) _{↑1.39}
DeBERTa _{base}	DeBERTa	89.33(1.05)	83.74(1.64)	83.67(0.45)	80.78(0.41)
	DAGCN	89.49(0.30) _{↑0.16}	84.25(0.42) _{↑0.51}	84.46(0.65) _{↑0.79}	81.66(0.50) _{↑0.88}
	TextGT	89.97(0.31) _{↑0.64}	85.30(0.38) _{↑1.56}	84.84(0.51) _{↑1.17}	82.33(0.66) _{↑1.55}
	MLFM	89.63(0.61) _{↑0.30}	84.62(0.79) _{↑0.88}	84.59(1.10) _{↑0.92}	81.73(1.22) _{↑0.95}
	GHI(ours)	90.33(0.49) _{↑1.00}	85.65(0.77) _{↑1.91}	85.06(0.70) _{↑1.39}	82.63(0.71) _{↑1.85}

Table 2: Controlled comparison under unified settings on SemEval-2014 domains. All results are reported as mean (standard deviation) over 5 seeds. Models above are all implemented by us.

3.3 Ablations

Table 3 presents the ablation results of GHI. On the SemEval-2014 domains, w/o Incidence Attention or w/o Hyperedge Nodes yield the most severe drops. Specifically, w/o Incidence Attention causes the largest accuracy decrease on both datasets, and reduces Macro-F1 by 2.68% on Restaurant14. In parallel, w/o Hyperedge Nodes proves most harmful to Laptop, reducing its Macro-F1 by 3.35%. These results suggest that token-hyperedge relations should not be treated merely as transient aggregation paths. Incidence Attention provides relation-aware token-hyperedge routing, allowing the model to distinguish deterministic syntactic links from softer semantic memberships. Mean-

while, the drop caused by removing Hyperedge Nodes supports the motivation of lifting structural priors into explicit reasoning nodes, where token-hyperedge and hyperedge-hyperedge interactions can be modeled directly.

The degradation pattern shifts significantly on the Twitter dataset. Unlike formal SemEval domains, Twitter texts are typically shorter, highly informal, and syntactically noisy, which severely diminishes the reliability of parser-derived fixed dependency priors. In this setting, removing Adaptive Hyperedges incurs the largest performance penalty. This suggests that sample-specific semantic clusters, dynamically induced from token and anchor states, become the decisive factor when explicit

Model	Restaurant14		Laptop		Twitter	
	Acc	F1	Acc	F1	Acc	F1
GHI	90.97	86.40	86.08	83.74	78.73	77.72
w/o Adaptive Hyperedges	90.08	85.25	84.49	81.60	75.63	74.81
w/o Hyperedge Nodes	89.45	84.14	84.18	80.39	75.63	74.99
w/o Incidence Attention	88.29	83.72	84.02	80.94	76.96	76.05
w/o Graphormer Structural Bias	89.37	83.87	84.18	81.58	76.22	75.95

Table 3: Ablation results. The variants remove adaptive hyperedges, explicit hyperedge nodes, Relation-Aware Incidence Attention in Eq. 4, or Graphormer structural biases \mathcal{B}^l in Eq. 5, respectively.

Method	Restaurant14	Laptop
BERTAsp+SCAPT(Li et al., 2021b)	72.28	77.59
DeBERTa+SPC [♣]	73.72	77.26
ABSA-ESA(Ouyang et al., 2024b)	73.76	77.91
GPT3+THOR(Fei et al., 2023)	76.55	73.12
Flan-T5+Prompt(11B)(Fei et al., 2023)	75.10	78.91
Flan-T5+THOR(11B)(Fei et al., 2023)	79.73	82.43
DeBERTa+GHI(ours, 247M)	79.64	81.96

Table 4: ISE Macro-F1 results. ♣ denotes baseline results implemented by us.

syntactic regularities are weak.

3.4 Implicit Sentiment Evaluation

Table 4 evaluates GHI on the Implicit Sentiment Eval (ISE) benchmark (Li et al., 2021b), a notoriously difficult setting where sentences lack explicit opinion words (e.g., "The battery lasts only 2 hours."). With only 247M parameters, the DeBERTa-based GHI yields an F1 score of 79.64% on Restaurant14 and 81.96% on Laptop, closely approaching the 11B-parameter Flan-T5+THOR (Fei et al., 2023), a method specifically prompted for multi-step chain-of-thought reasoning. Furthermore, GHI outperforms other heavy-weight baselines, including GPT3+THOR and standard Flan-T5 prompting. These results suggest that the proposed incidence-based reasoning provides competitive implicit-sentiment modeling without relying on large prompted language models.

3.5 Aspect Robustness Test

To evaluate the robustness of GHI in the face of textual adversarial attacks, we employ existing adversarial attack datasets, specifically Laptop14-ARTS and Restaurant14-ARTS (Xing et al., 2020). Table 5 presents results on the ARTS benchmark. GHI achieves the best Macro-F1 on two datasets, improving over strong LSAE (Yang and Li, 2024) by 3.32% and 4.33%, respectively, underscoring

Method	Restaurants14-ARTS		Laptop14-ARTS	
	Acc	F1	Acc	F1
DeBERTa*	74.97	66.48	67.71	65.60
CEIB(Chang et al., 2024)	80.00	73.97	69.18	65.51
LSAT(Yang and Li, 2024)	80.31	71.37	73.58	69.28
LSAP(Yang and Li, 2024)	81.19	72.54	73.34	68.46
LSAE(Yang and Li, 2024)	81.55	72.95	74.47	69.79
GHI(ours)	81.08	76.27	76.13	74.12

Table 5: Aspect Robustness Test results. Scores by model with * are copied from Yang and Li (2024).

the robustness of GHI under challenging settings.

3.6 Analysis and Visualization

Figure 4 summarizes the relative positions of tokens retained by adaptive Top- K incidence. The four bins denote tokens inside the aspect span, within 1–2 tokens, 3–5 tokens, and beyond 5 tokens, respectively. The retained tokens are mainly concentrated around the aspect span and its near context, while Laptop keeps more middle and long range tokens than Restaurant14. This result indicates that adaptive hyperedges select different evidence ranges across datasets under the same adaptive topology.

Figure 5 presents two illustrative cases to show how GHI organizes aspect-relevant evidence. Orange boxes indicate the hard Top- K tokens retained for the sparse adaptive topology. In both examples, GHI assigns higher weights to informative evidence regions. Notably, in the first case, the adaptive incidence for "food" assigns high weights to distant opinion evidence such as "simple" and "satisfying", suggesting that adaptive hyperedges can group aspect-relevant evidence across a broader context through learned incidence patterns. Furthermore, in the second case, for aspect "Startup times", GHI does not rely on the explicit modifier "long", but assigns stronger weights to the concrete temporal evidence "two minutes". This indicates

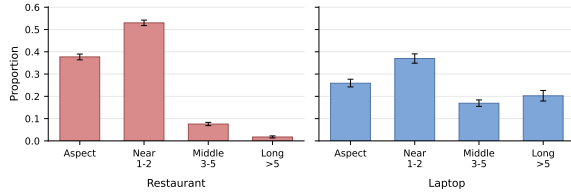


Figure 4: Distance distribution of adaptive Top-K tokens relative to aspect spans on SemEval-14 domains. Error bars denote 95% bootstrap confidence intervals.

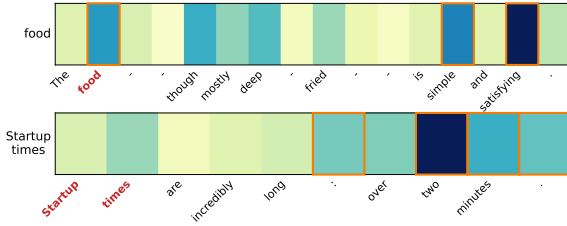


Figure 5: Visualization examples in two cases

that the learned incidence can capture multi-token and even implicit evidence expressions toward the target aspect.

4 Related Work

Structural modeling remains important for ABSA, where models must bind sentiment evidence to the correct aspect. Recent methods refine syntactic, semantic, and aspect-specific structures from different perspectives.

Early efforts in this direction, such as Zeng et al. (2019), pioneered local attention approaches via LCF mechanism. Building upon this, recognizing that sentiment reasoning cannot only rely on a narrow local window, Jin et al. (2025) expands this mechanism by fusing semantic and syntactic information through aspect-centered and hierarchical attentions.

Moving beyond optimizations restricted to purely sequential text methods like localized windows, graph-based modeling has emerged as a mainstream paradigm for structural representation. To effectively integrate local mechanisms into graph structures, Wang et al. (2024) filters noisy dependency edges with Distance-based Syntactic Weight and Aspect-Fusion Attention. To bridge these graphical structures with powerful global attention, Yin and Zhong (2024) couples a GNN-based graph view with a Transformer-based sequence view.

While traditional graphs effectively capture pairwise syntax, hypergraph-based ABSA further ex-

plores high-order relations beyond pairwise dependency edges. Ouyang et al. (2024a) builds word-level relational hypergraphs from syntactic and semantic relations and applies aspect-specific hypergraph attention, while Kashyap et al. (2025) induces dynamic aspect-opinion hyperedges through sample-specific hierarchical clustering. These works suggest that hyperedges are suitable for representing multi-token sentiment evidence.

Expanding the scope from ABSA-specific architectures, graph representation learning has continued to evolve beyond localized message passing. Graphormer shows that structural encodings can be injected into Transformer attention, allowing global graph-aware interaction beyond local message passing (Ying et al., 2021). Once hyperedges are lifted into nodes, token–token, token–hyperedge, and hyperedge–hyperedge relations can be modeled in the same attention space. Recent adaptive hypergraph designs outside NLP, such as HyperACE in YOLOv13, also highlight the potential of dynamically induced high-order correlations (Lei et al., 2025).

To rigorously test these diverse modeling approaches, recent studies have introduced more challenging evaluation settings for sentiment reasoning. Fei et al. (2023) study implicit sentiment through multi-hop reasoning over implicit aspects, opinions, and polarities. Yang and Li (2024) evaluate robustness on ARTS (Xing et al., 2020), where distracting sentiment words and aspect-opinion mismatches expose reliance on global sentiment shortcuts. These benchmarks test whether models can reliably bind evidence under implicit, noisy, or adversarial conditions, and are therefore useful for evaluating the reliability of incidence-based structural reasoning.

5 Conclusion

In this paper, we proposed GHI, a Graphormer-over-conditioned-Hypergraph-Incidence framework for ABSA. GHI converts heterogeneous linguistic and semantic evidence into token–hyperedge incidence relations, avoiding source-specific reasoning branches while retaining explicit structural control. Through soft incidence propagation and hard incidence bipartite star-expanded Graphormer attention, the framework reasons jointly over diverse evidence in a shared space. Results across comprehensive datasets support the effectiveness of this incidence-centered design.

Limitations

GHI currently focuses on aspect-term sentiment classification, where the target aspect is given. It does not directly address aspect extraction, opinion extraction, or end-to-end aspect–opinion pair discovery. Extending the incidence formulation to full ABSA pipelines would require additional decoding mechanisms or supervision for inducing aspects, opinions, and their sentiment relations.

Second, the effectiveness of GHI can still be influenced by the quality of structural priors and the bounded hyperedge budget. Dependency-based hyperedges may inherit noise from parser outputs or preprocessing artifacts, while the fixed number of adaptive hyperedges and the Top- K hard incidence view may miss weak but useful associations in highly complex sentences.

Finally, the current star-expanded Graphormer uses dense attention over the expanded token–hyperedge graph. Although the bounded hyperedge budget keeps the overhead controlled for short ABSA texts, applying the same design to long reviews, documents, or dialogue-level sentiment analysis may require sparse attention or hierarchical incidence construction.

References

- Mingshan Chang, Min Yang, Qingshan Jiang, and Ruifeng Xu. 2024. [Counterfactual-enhanced information bottleneck for aspect-based sentiment analysis](#). *Proceedings of the AAAI Conference on Artificial Intelligence*, 38(16):17736–17744.
- Bingfeng Chen, Qihan Ouyang, Yongqi Luo, Boyan Xu, Ruichu Cai, and Zhifeng Hao. 2024. [S²GSL: Incorporating segment to syntactic enhanced graph structure learning for aspect-based sentiment analysis](#). In *Proceedings of the 62nd Annual Meeting of the Association for Computational Linguistics (Volume 1: Long Papers)*, pages 13366–13379, Bangkok, Thailand. Association for Computational Linguistics.
- Chenhua Chen, Zhiyang Teng, Zhongqing Wang, and Yue Zhang. 2022. [Discrete opinion tree induction for aspect-based sentiment analysis](#). In *Proceedings of the 60th Annual Meeting of the Association for Computational Linguistics (Volume 1: Long Papers)*, pages 2051–2064, Dublin, Ireland. Association for Computational Linguistics.
- Chenhua Chen, Zhiyang Teng, and Yue Zhang. 2020. [Inducing target-specific latent structures for aspect sentiment classification](#). In *Proceedings of the 2020 Conference on Empirical Methods in Natural Language Processing (EMNLP)*, pages 5596–5607, Online. Association for Computational Linguistics.
- Junqi Dai, Hang Yan, Tianxiang Sun, Pengfei Liu, and Xipeng Qiu. 2021. [Does syntax matter? a strong baseline for aspect-based sentiment analysis with RoBERTa](#). In *Proceedings of the 2021 Conference of the North American Chapter of the Association for Computational Linguistics: Human Language Technologies*, pages 1816–1829, Online. Association for Computational Linguistics.
- Li Dong, Furu Wei, Chuanqi Tan, Duyu Tang, Ming Zhou, and Ke Xu. 2014. [Adaptive recursive neural network for target-dependent Twitter sentiment classification](#). In *Proceedings of the 52nd Annual Meeting of the Association for Computational Linguistics (Volume 2: Short Papers)*, pages 49–54, Baltimore, Maryland. Association for Computational Linguistics.
- Hao Fei, Bobo Li, Qian Liu, Lidong Bing, Fei Li, and Tat-Seng Chua. 2023. [Reasoning implicit sentiment with chain-of-thought prompting](#). In *Proceedings of the 61st Annual Meeting of the Association for Computational Linguistics (Volume 2: Short Papers)*, pages 1171–1182, Toronto, Canada. Association for Computational Linguistics.
- Ao Feng, Jiazhi Cai, Zhengjie Gao, and Xiaojie Li. 2023. [Aspect-level sentiment classification with fused local and global context](#). *Journal of Big Data*, 10(1):176.
- Yifan Feng, Haoxuan You, Zizhao Zhang, Rongrong Ji, and Yue Gao. 2019. [Hypergraph neural networks](#). *Proceedings of the AAAI Conference on Artificial Intelligence*, 33(01):3558–3565.
- Pengcheng He, Xiaodong Liu, Jianfeng Gao, and Weizhu Chen. 2020. [Deberta: Decoding-enhanced BERT with disentangled attention](#). *CoRR*, abs/2006.03654.
- Jie Ji, Wenlong Zhu, Chengle Hou, Qiaoyan Song, YuKun Ma, and Youruo Wang. 2026. [Dagf: A dual gcn and auxiliary graph fusion based model for aspect-based sentiment analysis](#). *Applied Soft Computing*, 195:115040.
- Zhongquan Jian, Jiajian Li, Qingqiang Wu, and Junfeng Yao. 2024. [Retrieval contrastive learning for aspect-level sentiment classification](#). *Information Processing & Management*, 61(1):103539.
- Zhongquan Jian, Daihang Wu, Shaopan Wang, Yancheng Wang, Junfeng Yao, Meihong Wang, and Qingqiang Wu. 2025. [AGCL: Aspect graph construction and learning for aspect-level sentiment classification](#). In *Proceedings of the 31st International Conference on Computational Linguistics*, pages 841–854, Abu Dhabi, UAE. Association for Computational Linguistics.
- Qingnan Jiang, Lei Chen, Ruifeng Xu, Xiang Ao, and Min Yang. 2019. [A challenge dataset and effective models for aspect-based sentiment analysis](#). In *Proceedings of the 2019 Conference on Empirical Methods in Natural Language Processing and the*

- 9th International Joint Conference on Natural Language Processing (EMNLP-IJCNLP), pages 6280–6285, Hong Kong, China. Association for Computational Linguistics.
- Song Jin, Qing He, Yuji Wang, Nisuo Du, and Wenjing Lei. 2025. [Aspect-based sentiment analysis with semantic and syntactic enhanced multi-layer fusion model](#). *Engineering Applications of Artificial Intelligence*, 159:111654.
- Xinyi Ju, Ling Ding, Ru Yang, Chang Guo, Guojian Zou, Bo Zhang, and Meizi Li. 2025. [Dual contrastive learning-based hypergraph convolutional network for aspect-based sentiment classification](#). *Knowledge-Based Systems*, 330:114701.
- Omkar Mahesh Kashyap, Padegal Amit, Madhav Kashyap, Ashwini M Joshi, and Shylaja SS. 2025. [From graphs to hypergraphs: Enhancing aspect-based sentiment analysis via multi-level relational modeling](#). *Preprint*, arXiv:2511.14142.
- Mengqi Lei, Siqi Li, Yihong Wu, Han Hu, You Zhou, Xihu Zheng, Guiguang Ding, Shaoyi Du, Zongze Wu, and Yue Gao. 2025. [Yolov13: Real-time object detection with hypergraph-enhanced adaptive visual perception](#). *Preprint*, arXiv:2506.17733.
- Ruifan Li, Hao Chen, Fangxiang Feng, Zhanyu Ma, Xiaojie Wang, and Eduard Hovy. 2021a. [Dual graph convolutional networks for aspect-based sentiment analysis](#). In *Proceedings of the 59th Annual Meeting of the Association for Computational Linguistics and the 11th International Joint Conference on Natural Language Processing (Volume 1: Long Papers)*, pages 6319–6329, Online. Association for Computational Linguistics.
- Zhengyan Li, Yicheng Zou, Chong Zhang, Qi Zhang, and Zhongyu Wei. 2021b. [Learning implicit sentiment in aspect-based sentiment analysis with supervised contrastive pre-training](#). In *Proceedings of the 2021 Conference on Empirical Methods in Natural Language Processing*, pages 246–256, Online and Punta Cana, Dominican Republic. Association for Computational Linguistics.
- Fukun Ma, Xuming Hu, Aiwei Liu, Yawen Yang, Shuang Li, Philip S. Yu, and Lijie Wen. 2023. [AMR-based network for aspect-based sentiment analysis](#). In *Proceedings of the 61st Annual Meeting of the Association for Computational Linguistics (Volume 1: Long Papers)*, pages 322–337, Toronto, Canada. Association for Computational Linguistics.
- Rajdeep Mukherjee, Shreyas Shetty, Subrata Chattopadhyay, Subhadeep Maji, Samik Datta, and Pawan Goyal. 2021. [Reproducibility, replicability and beyond: Assessing production readiness of aspect based sentiment analysis in the wild](#). In *Advances in Information Retrieval*, pages 92–106, Cham. Springer International Publishing.
- Jihong Ouyang, Chang Xuan, Bing Wang, and Zhiyao Yang. 2024a. [Aspect-based sentiment classification with aspect-specific hypergraph attention networks](#). *Expert Systems with Applications*, 248:123412.
- Jihong Ouyang, Zhiyao Yang, Silong Liang, Bing Wang, Yimeng Wang, and Ximing Li. 2024b. [Aspect-based sentiment analysis with explicit sentiment augmentations](#). *Proceedings of the AAAI Conference on Artificial Intelligence*, 38(17):18842–18850.
- Maria Pontiki, Dimitris Galanis, Haris Papageorgiou, Ion Androutsopoulos, Suresh Manandhar, Mohammad AL-Smadi, Mahmoud Al-Ayyoub, Yanyan Zhao, Bing Qin, Orphée De Clercq, Véronique Hoste, Marianna Apidianaki, Xavier Tannier, Natalia Loukachevitch, Evgeniy Kotelnikov, Nuria Bel, Salud María Jiménez-Zafra, and Gülşen Eryiğit. 2016. [SemEval-2016 task 5: Aspect based sentiment analysis](#). In *Proceedings of the 10th International Workshop on Semantic Evaluation (SemEval-2016)*, pages 19–30, San Diego, California. Association for Computational Linguistics.
- Maria Pontiki, Dimitris Galanis, Haris Papageorgiou, Suresh Manandhar, and Ion Androutsopoulos. 2015. [SemEval-2015 task 12: Aspect based sentiment analysis](#). In *Proceedings of the 9th International Workshop on Semantic Evaluation (SemEval 2015)*, pages 486–495, Denver, Colorado. Association for Computational Linguistics.
- Maria Pontiki, Dimitris Galanis, John Pavlopoulos, Haris Papageorgiou, Ion Androutsopoulos, and Suresh Manandhar. 2014. [SemEval-2014 task 4: Aspect based sentiment analysis](#). In *Proceedings of the 8th International Workshop on Semantic Evaluation (SemEval 2014)*, pages 27–35, Dublin, Ireland. Association for Computational Linguistics.
- Hao Tang, Donghong Ji, Chenliang Li, and Qiji Zhou. 2020. [Dependency graph enhanced dual-transformer structure for aspect-based sentiment classification](#). In *Proceedings of the 58th Annual Meeting of the Association for Computational Linguistics*, pages 6578–6588, Online. Association for Computational Linguistics.
- Yuanhe Tian, Guimin Chen, and Yan Song. 2021. [Aspect-based sentiment analysis with type-aware graph convolutional networks and layer ensemble](#). In *Proceedings of the 2021 Conference of the North American Chapter of the Association for Computational Linguistics: Human Language Technologies*, pages 2910–2922, Online. Association for Computational Linguistics.
- Bo Wang, Tao Shen, Guodong Long, Tianyi Zhou, and Yi Chang. 2021. [Eliminating sentiment bias for aspect-level sentiment classification with unsupervised opinion extraction](#). In *Findings of the Association for Computational Linguistics: EMNLP 2021*, pages 3002–3012, Punta Cana, Dominican Republic. Association for Computational Linguistics.
- Kai Wang, Weizhou Shen, Yunyi Yang, Xiaojun Quan, and Rui Wang. 2020. [Relational graph attention net-](#)

- work for aspect-based sentiment analysis. In *Proceedings of the 58th Annual Meeting of the Association for Computational Linguistics*, pages 3229–3238, Online. Association for Computational Linguistics.
- Zhihao Wang, Bo Zhang, Ru Yang, Chang Guo, and Maozhen Li. 2024. DAGCN: Distance-based and aspect-oriented graph convolutional network for aspect-based sentiment analysis. In *Findings of the Association for Computational Linguistics: NAACL 2024*, pages 1863–1876, Mexico City, Mexico. Association for Computational Linguistics.
- Xiaoyu Xing, Zhijing Jin, Di Jin, Bingning Wang, Qi Zhang, and Xuanjing Huang. 2020. Tasty burgers, soggy fries: Probing aspect robustness in aspect-based sentiment analysis. In *Proceedings of the 2020 Conference on Empirical Methods in Natural Language Processing (EMNLP)*, pages 3594–3605, Online. Association for Computational Linguistics.
- Heng Yang and Ke Li. 2024. Modeling aspect sentiment coherency via local sentiment aggregation. In *Findings of the Association for Computational Linguistics: EACL 2024*, pages 182–195, St. Julian’s, Malta. Association for Computational Linguistics.
- Heng Yang, Chen Zhang, and Ke Li. 2023. Pyabsa: A modularized framework for reproducible aspect-based sentiment analysis. In *Proceedings of the 32nd ACM International Conference on Information and Knowledge Management, CIKM ’23*, page 5117–5122, New York, NY, USA. Association for Computing Machinery.
- Shuo Yin and Guoqiang Zhong. 2024. Textgt: A double-view graph transformer on text for aspect-based sentiment analysis. *Proceedings of the AAAI Conference on Artificial Intelligence*, 38(17):19404–19412.
- Chengxuan Ying, Tianle Cai, Shengjie Luo, Shuxin Zheng, Guolin Ke, Di He, Yanming Shen, and Tie-Yan Liu. 2021. Do transformers really perform badly for graph representation? In *Advances in Neural Information Processing Systems*, volume 34, pages 28877–28888. Curran Associates, Inc.
- Bengong Yu and Shuwen Zhang. 2023. A novel weight-oriented graph convolutional network for aspect-based sentiment analysis. *The Journal of Supercomputing*, 79(1):947–972.
- Biqing Zeng, Heng Yang, Ruyang Xu, Wu Zhou, and Xuli Han. 2019. Lcf: A local context focus mechanism for aspect-based sentiment classification. *Applied Sciences*, 9(16).
- Chen Zhang, Qiuchi Li, and Dawei Song. 2019. Syntax-aware aspect-level sentiment classification with proximity-weighted convolution network. In *Proceedings of the 42nd International ACM SIGIR Conference on Research and Development in Information Retrieval, SIGIR’19*, page 1145–1148, New York, NY, USA. Association for Computing Machinery.
- Wenxuan Zhang, Xin Li, Yang Deng, Lidong Bing, and Wai Lam. 2023. A survey on aspect-based sentiment analysis: Tasks, methods, and challenges. *IEEE Transactions on Knowledge and Data Engineering*, 35(11):11019–11038.
- Zheng Zhang, Zili Zhou, and Yanna Wang. 2022. SSEGCN: Syntactic and semantic enhanced graph convolutional network for aspect-based sentiment analysis. In *Proceedings of the 2022 Conference of the North American Chapter of the Association for Computational Linguistics: Human Language Technologies*, pages 4916–4925, Seattle, United States. Association for Computational Linguistics.
- Jie Zhou, Jimmy Xiangji Huang, Qinmin Vivian Hu, and Liang He. 2020. Sk-gcn: Modeling syntax and knowledge via graph convolutional network for aspect-level sentiment classification. *Knowledge-Based Systems*, 205:106292.

A Experimental Details

A.1 Datasets

We conduct experiments on six standard benchmark datasets on ABSA. The statistics of the six datasets are shown in Table 6. Restaurant14 and Laptop datasets are from SemEval-2014 Task 4 (Pontiki et al., 2014). Twitter dataset is the target-dependent Twitter sentiment corpus introduced by Dong et al. (2014). Restaurant15 and Restaurant16 datasets are from the restaurant-domain subsets of SemEval-2015 Task 12 and SemEval-2016 Task 5, respectively (Pontiki et al., 2015, 2016). MAMS is the Multi-Aspect Multi-Sentiment dataset introduced by Jiang et al. (2019), where each sentence contains multiple aspects with different sentiment polarities. All datasets are used for research purposes, following their original licenses and distribution terms.

For ISE, we follow prior implicit-sentiment evaluation protocols and process all instances using the same dependency parsing and token-alignment pipelines as in the main experiments. For ARTS, we follow the adversarial aspect robustness evaluation protocol. Models are trained only on the original training split, without ARTS augmentation. The models are evaluated directly on the perturbed ARTS test samples.

A.2 Implementation Details

We use DeBERTa-v3-base as the pre-trained encoder and feed the sentence–aspect pair as encoder input. Word-level dependency parses are aligned to subword-level encoder states before graph construction. The model is optimized with

Dataset	Split	Positive	Neutral	Negative
Restaurant14	Train	2164	637	807
	Test	727	196	196
Laptop	Train	976	455	851
	Test	337	167	128
Twitter	Train	1507	3016	1528
	Test	172	336	169
Restaurant15	Train	912	36	256
	Test	326	34	182
Restaurant16	Train	1240	69	439
	Test	469	30	117
MAMS	Train	3380	5042	2764
	Val	403	604	325
	Test	400	607	329

Table 6: Statistics of the six standard benchmark datasets.

AdamW using a batch size of 16 and gradient clipping of 1.0. The learning rate is selected from $\{1 \times 10^{-5}, 2 \times 10^{-5}, 2.5 \times 10^{-5}\}$, and the weight decay is selected from $\{1 \times 10^{-4}, 5 \times 10^{-3}\}$. We train for 30 epochs on six standard benchmark datasets.

For GHI, we use 2 reasoning layers. The static hyperedges include aspect, SRD-based local-context, and dependency hyperedges, with dependency hop threshold $T = 2$. The local window size is selected from $\{3, 4\}$, the SRD radius from $\{3, 5\}$, and the adaptive Top- K from $\{3, 4\}$. The number of adaptive hyperedges is set to $M = 6$ for Twitter and $M = 4$ for the rest. All experiments are conducted on a single NVIDIA RTX 5080 GPU.

A.3 Additional Multi-seed Results on Twitter

We additionally report multi-seed results on Twitter, as shown in Table 7. On the noisier Twitter domain, GHI obtains modest but consistent gains over the vanilla DeBERTa-base encoder, suggesting that the incidence reasoning layer is not limited to the cleaner SemEval-2014 domains.

B Framework Details

B.1 Adaptive Hyperedges Generation

Let $P^0 \in \mathbb{R}^{M \times d_h}$ denote M learnable base adaptive hyperedge prototypes, where d_h denotes the hidden dimension. They are randomly initialized as global parameters and shared by all samples and reasoning layers, serving as the latent bases from which adaptive hyperedges are induced.

At each reasoning layer, GHI conditions these shared prototypes on the current sentence and as-

Model	Twitter	
	Acc	F1
DeBERTa	77.99(0.38)	77.24(0.32)
GHI(ours)	78.31(0.38)	77.46(0.26)

Table 7: Additional controlled comparison against vanilla DeBERTa-base on Twitter. Results are reported as mean(std) over 5 seeds.

pect anchors to induce sample-specific adaptive hyperedges. We first summarize the current instance by:

$$g^\ell = [c^\ell; a^\ell; \text{Pool}_m(\tilde{H}^\ell)], \quad (9)$$

where $\text{Pool}_m(\cdot)$ mean-pools valid sentence tokens. The context vector g^ℓ is mapped to a prototype offset $\Delta P^\ell \in \mathbb{R}^{M \times d}$, which is then used to generate the context-conditioned adaptive prototypes P_j^ℓ :

$$\Delta P^\ell = \text{reshape}(\text{MLP}(g^\ell)), \quad (10)$$

$$P_j^\ell = \text{LN}(P_j^0 + \Delta P_j^\ell + a^\ell), \quad j = 1, \dots, M, \quad (11)$$

where the aspect anchor is added to each prototype as a target-specific bias. Thus, sentence anchor c^ℓ , aspect anchor a^ℓ , and the pooled token context \tilde{H}^ℓ adapt the shared bases P^0 to the current instance.

For each conditioned adaptive hyperedge prototype, GHI computes token-prototype participation scores for token $i \in V$ and prototype $j = 1, \dots, M$:

$$s_{ij}^\ell = \frac{\langle W_t \tilde{H}_i^\ell, W_p P_j^\ell \rangle}{\sqrt{d_k}} + \frac{\langle W_a \tilde{H}_i^\ell, a^\ell \rangle}{\sqrt{d_k}}, \quad (12)$$

where W_t , W_p , and W_a are learned projections from tokens, prototypes and aspects, respectively. The d_k denotes the projection dimension used for scaling.

The soft adaptive incidence is obtained by applying a masked softmax over valid graph-visible tokens for each prototype:

$$I_{ad,ij}^\ell = \text{MaskedSoftmax}_i(s_{ij}^\ell; m), \quad (13)$$

where $I_{ad,ij}^\ell$ is the normalized incidence weight between token i and the adaptive hyperedge induced by prototype j , and the mask m excludes

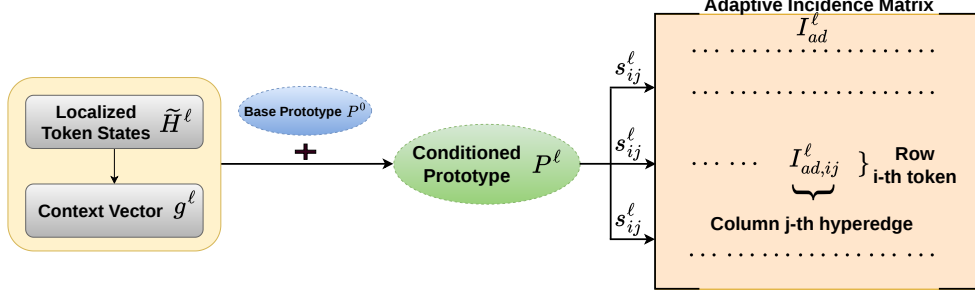


Figure 6: Adaptive Incidence Generation

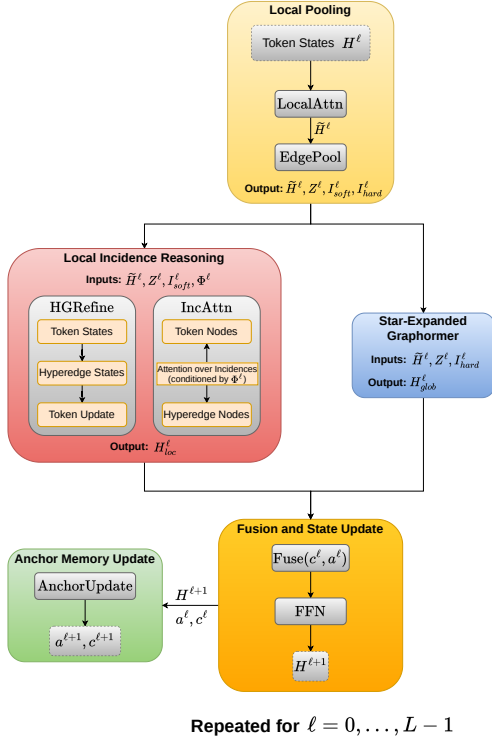


Figure 7: Layer-wise propagation in one GHI reasoning layer.

invalid tokens from the normalization. Together with the prototype conditioning in Eqs. 9–12, this masked-softmax normalization instantiates $\text{AdaptiveIncidence}(\cdot)$ in Eq. 2.

Finally, each conditioned prototype generates one adaptive hyperedge, and the M generated hyperedges form $I_{ad}^\ell \in \mathbb{R}^{|V| \times M}$. The overall generation process is illustrated in Figure 6.

B.2 Layer-Wise Computation Flow

As shown in Figure 7, starting from token states H^ℓ , local-window attention produces \tilde{H}^ℓ , edge pooling produces hyperedge states Z^ℓ and soft/hard incidence matrices. GHI then performs local inci-

dence reasoning through HGRefine and IncAttn in parallel with star-expanded Graphormer reasoning, followed by anchor-conditioned fusion and a feed-forward update to obtain $H^{\ell+1}$. Anchor memories are updated from $H^{\ell+1}$ for the next layer. The details of the HGRefine, IncAttn and AnchorUpdate are as follows.

HGRefine Given the soft incidence matrix I_{soft}^ℓ , HGRefine performs incidence-weighted token-hyperedge propagation. We first column-normalize incidence weights over tokens for each hyperedge:

$$\alpha_{ij}^\ell = \frac{I_{soft,ij}^\ell}{\sum_{i'} I_{soft,i'j}^\ell}, \quad (14)$$

and update hyperedge states by aggregating token states:

$$\hat{Z}_j^\ell = \sum_i \alpha_{ij}^\ell W_t \tilde{H}_i^\ell. \quad (15)$$

The updated hyperedge states are then written back to tokens using row-normalized incidence weights β_{ij}^ℓ over hyperedges:

$$\beta_{ij}^\ell = \frac{I_{soft,ij}^\ell}{\sum_{j'} I_{soft,ij'}^\ell}, \quad (16)$$

$$v_i^\ell = W_o \sum_j \beta_{ij}^\ell \hat{Z}_j^\ell. \quad (17)$$

The vector v_i^ℓ is the HGRefine message for token i in Eq. 4.

IncAttn IncAttn further performs token-hyperedge attention with incidence-level relation features. For token i and hyperedge j , we construct relation feature Φ_{ij}^ℓ from edge type, edge role (static and adaptive), incidence weight, token SRD, and hyperedge SRD. For attention head r , IncAttn computes an attention logit $e_{ij}^{\ell,r}$ that measures how strongly token i attends to hyperedge j :

$$e_{ij}^{\ell,r} = \frac{\langle W_Q^r \tilde{H}_i^\ell, W_K^r Z_j^\ell \rangle}{\sqrt{d_k}} + b_r(\Phi_{ij}^\ell) + \log(I_{\text{soft},ij}^\ell + \epsilon), \quad (18)$$

where W_Q^r and W_K^r are the query and key projections for attention head r , d_k is the projected key dimension, $b_r(\Phi_{ij}^\ell)$ is the relation-aware attention bias, and ϵ is a small constant for numerical stability. The logarithmic term injects the soft incidence weight as a prior attention bias.

The attention weights are then obtained by masked softmax over valid hyperedges:

$$a_{ij}^{\ell,r} = \text{MaskedSoftmax}_j(e_{ij}^{\ell,r}). \quad (19)$$

To modulate the value passed from each hyperedge, IncAttn further computes a scalar relation-aware gate:

$$\gamma_{ij}^\ell = \sigma(W_\gamma \Phi_{ij}^\ell + b_\gamma), \quad (20)$$

where W_γ and b_γ are learned parameters that map the relation feature Φ_{ij}^ℓ to a scalar value gate. This gate controls how much the hyperedge j contributes to the IncAttn message of token i .

The IncAttn message for token i is then computed by aggregating gated hyperedge values across attention heads r :

$$q_i^\ell = W_o \text{Concat}_r \sum_j a_{ij}^{\ell,r} \gamma_{ij}^\ell W_V^r Z_j^\ell. \quad (21)$$

Here, W_V^r is the value projection for head r , W_o is the output projection, and Concat_r concatenates the outputs of all heads r . The resulting q_i^ℓ is the IncAttn message added to the token update in Eq. 4.

AnchorUpdate After obtaining $H^{\ell+1}$, GHI updates the sentence and aspect anchors by gated residual MLPs. Let $\bar{H}^{\ell+1} = \text{Pool}_m(H^{\ell+1})$ and $\bar{a}^{\ell+1} = \text{Pool}_{[l,r]}(H^{\ell+1})$. We form:

$$u_c^\ell = [c^\ell; a^\ell; \bar{h}^{\ell+1}], \quad (22)$$

$$u_a^\ell = [a^\ell; c^\ell; \bar{a}^{\ell+1}], \quad (23)$$

and update the anchor as:

$$c^{\ell+1} = c^\ell + \sigma(W_c u_c^\ell) \odot \text{MLP}_c(u_c^\ell), \quad (24)$$

$$a^{\ell+1} = a^\ell + \sigma(W_a u_a^\ell) \odot \text{MLP}_a(u_a^\ell). \quad (25)$$

These updated anchors are used for next-layer incidence induction and local-global fusion.

C Sensitivity Analyses

We further examine the sensitivity of GHI to three structural hyperparameters: the adaptive Top- K used for constructing the sparse hard incidence topology, the number of adaptive hyperedges M , and the number of GHI reasoning layers L . We conduct the analysis on three representative datasets, Restaurant14, Laptop, and Twitter. For each study, we vary one hyperparameter from 1 to 6 while keeping the remaining settings fixed to the main configuration of the corresponding dataset.

Figure 8 shows the results of the sensitivity experiments. For adaptive Top- K , moderate values generally perform better, suggesting that the hard topology benefits from retaining several high-order token representations. For the number of adaptive hyperedges M , performance usually saturates with a small number, indicating that a compact set of sample-specific evidence slots is sufficient for ABSA. Meanwhile, increasing M further does not consistently improve performance and may introduce redundant or noisy memberships. For the number of reasoning layers L , GHI also performs well with shallow stacks, with $L = 2$ or nearby values often yielding strong results. This supports our design choice of using compact incidence reasoning instead of relying on deep graph stacking.

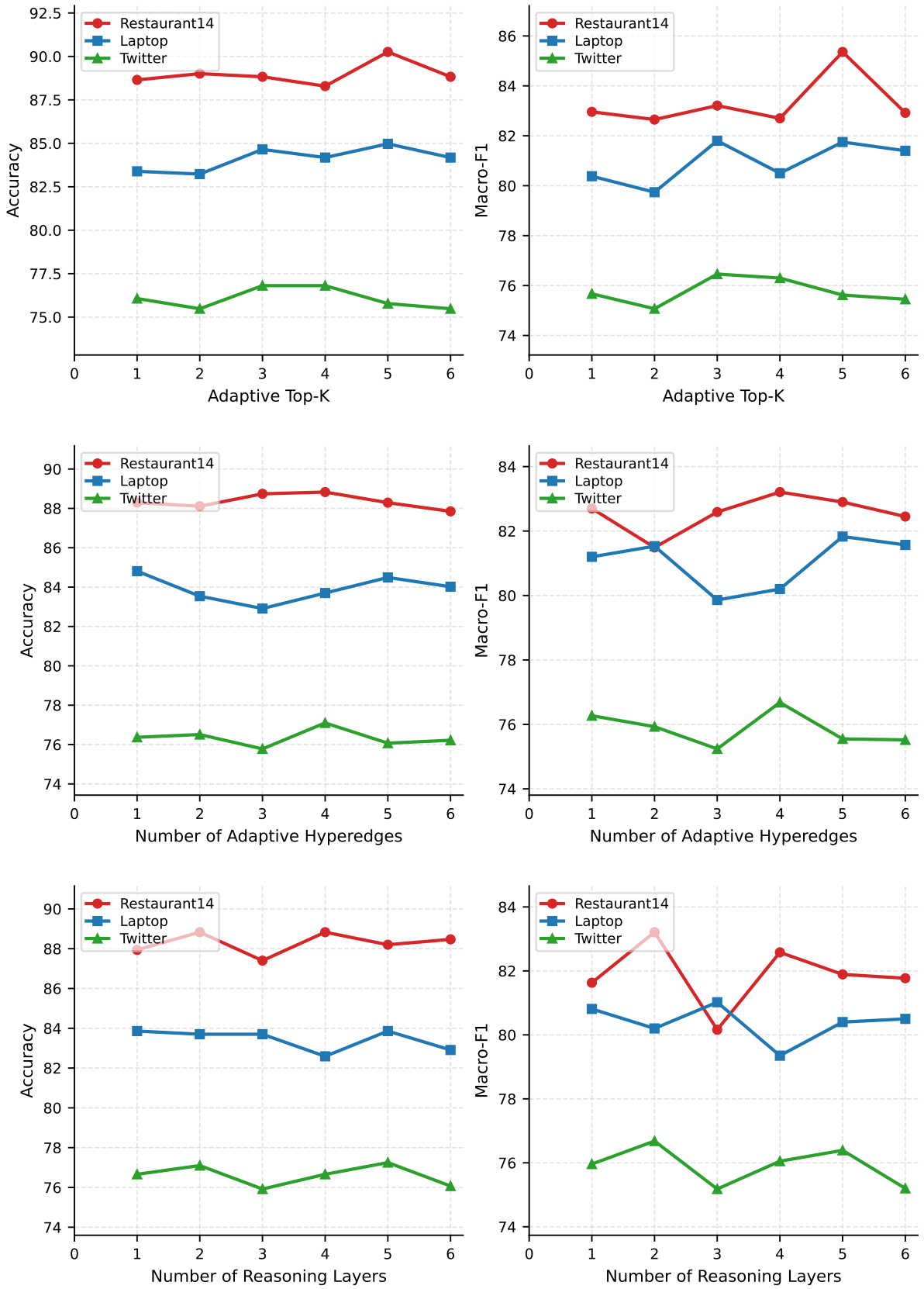


Figure 8: Sensitivity analyses for number of Adaptive Top- K , number of adaptive hyperedges M , and number of GHI layers L , respectively.